Integrating superconducting phase and topological crystalline quantum spin Hall effect in hafnium intercalated gallium film

Jian Zhou,[1,a)] Shunhong Zhang,[2] Qian Wang,[2,1] and Puru Jena[1,a)]
[1]*Department of Physics, Virginia Commonwealth University, Richmond, Virginia 23284, USA*
[2]*Center for Applied Physics and Technology, College of Engineering, Peking University, Beijing 100871, China*

(Received 25 April 2016; accepted 5 June 2016; published online 20 June 2016)

Motivated by the growth of superconducting atomic hexagonal Ga layers on GaN surface we have calculated the electronic properties of Hf intercalated honeycomb Ga layers using first-principles theory. In contrast to the hexagonal Ga layers where substrate is necessary for their stability, we find the above structure to be dynamically stable in its freestanding form with small formation energy. In particular, six Dirac cones composed of Hf-$d_{xy}/d_{x2\text{-}y2}$ orbitals are observed in the first Brillouin zone, slightly below the Fermi energy. Spin-orbit coupling opens a large band gap of 177 meV on these Dirac cones. By calculating its mirror Chern number, we demonstrate that this band gap is topologically nontrivial and protected by mirror symmetry. Such mirror symmetry protected band gaps are rare in hexagonal lattice. A large topological crystalline quantum spin Hall conductance $\sigma_{SH} \sim -4\ e^2/h$ is also revealed. Moreover, electron-phonon coupling calculations reveal that this material is superconducting with a transition temperature $T_c = 2.4$ K, mainly contributed by Ga out-of-plane vibrations. Our results provide a route toward manipulating quantum spin Hall and superconducting behaviors in a single material which helps to realize Majorana fermions and topological superconductors. *Published by AIP Publishing.*
[http://dx.doi.org/10.1063/1.4954672]

Two-dimensional (2D) quantum spin Hall (QSH) materials and superconductors are of considerable current interest because of their importance in understanding fundamental problems in condensed matter physics as well as for their potential practical applications in future nanoelectronic devices. Both materials feature dissipationless conduction electrons. The former (QSH), exhibiting metallic bands without back scattering on its edge, is usually seen in 2D topologically nontrivial materials such as topological insulator (TI),[1] which is protected by time-reversal symmetry. Besides, recently another class of topological materials has been predicted and observed whose electronic topology is protected by crystal symmetries.[2–5] These materials, so-called 2D topological crystalline insulators (TCI), also possess spin polarized electric current along their edges. Up to now, many 2D TCIs have been proposed, and most of them appear in *square* lattice structures. The 2D superconductors, on the other hand, enable scientists to understand electron pairing mechanisms and enhance the superconducting transition temperature T_c. The recent discovery of 2D superconductors in electrically gated MoS_2[6] and Li adsorbed graphene[7,8] also provide sufficient evidence for controlling electron pairing in quantum confined systems. It would be interesting if both 2D topologically nontrivial QSH and superconducting behaviors can be integrated in a *single* material. Such material will then serve as a platform to realize Majorana fermions and topological superconductors. However, thus far, achieving this goal remains elusive.

Gallium-based materials are a family of superconductors that are receiving great attention in recent years. For example, transition metal-embedded Ga materials belong to a class of molecular-based superconductors.[9] Very recently, Xue *et al.* have grown a hexagonal Ga thin film with a few atomic layers on GaN(0001) semiconductor surface.[10,11] They have shown that it becomes superconducting below 5 K.[10] Especially, they also observed a superconductor-metal transition with Griffiths singularity in a three-layer Ga film.[11] These findings open the door for exploring unusual physical behaviors of Ga-based thin films.

One obstacle in the Ga thin film is its instability in isolated state. Due to its incompatibility with the chemical aromatic rule, further discoveries and applications of these materials are hindered. So the question arises: can one stabilize a 2D Ga-based thin film in isolated form and if so does it have unusual properties such as superconductivity and/or QSH effect? In this letter, using first-principles calculations we predict an Hf intercalated honeycomb (*h*-) Ga film which is dynamically stable in its freestanding form. Note that a single layer of Hf sheet has also been fabricated on Ir(111) surface.[12] This intercalated structure has mirror symmetry about the *z*-plane. Our electronic structure calculations demonstrate that six Dirac-like band crossings appear at 68 meV below the Fermi level (E_F) along the $\Gamma \rightarrow$ K path in the first Brillouin zone (BZ). Inclusion of spin-orbit coupling (SOC) interaction opens a large topologically nontrivial gap of 177 meV at these Dirac points. We also find a nearly quantized intrinsic QSH conductance $\sigma^{SH} \sim -4e^2/h$ within this gap. By calculating the mirror Chern number $C_M \equiv (C_{+i} - C_{-i})/2$, where C_{+i} and C_{-i} are the Chern numbers of Bloch states with opposite eigenvalues of a mirror operator M, we demonstrate that these band gaps are protected by mirror symmetry. Note that mirror symmetry protected 2D topological

[a)]Electronic addresses: jzhou2@vcu.edu and pjena@vcu.edu

crystalline phases are usually seen in square lattice. Our results provide a possible route to achieve it in hexagonal lattice. In addition, by performing electron-phonon coupling (EPC) calculations, this structure is found to be a Bardeen–Cooper–Schrieffer (BCS) superconductor with $T_c = 2.4$ K, comparable with previously reported Ga-based superconductors. In this regard, we combine intrinsic topological crystalline evoked QSH and BCS superconducting behaviors in a single 2D material, which can be tuned effectively by slightly shifting its chemical potential.

Our first-principles calculations are based on density functional theory (DFT) with generalized gradient approximation (GGA) for exchange-correlation functional proposed by Perdew–Burke–Ernzerhof (PBE).[13] All the geometric relaxation and electronic property calculations are calculated by using the Vienna *ab initio* simulation package (VASP).[14] The plane wave basis set with energy cutoff of 350 eV and the projector-augmented wave method[15] are used. We use a Γ-centered Monkhorst–Pack[16] k-mesh of $(15 \times 15 \times 1)$ to optimize the geometric structure, a k-mesh of $(25 \times 25 \times 1)$ to calculate the electronic properties, and a k-mesh of $(180 \times 180 \times 1)$ to compute and integrate the Berry curvatures. For the phonon dispersion and EPC parameters, we use the Quantum-ESPRESSO (QE) code,[17] with a k-mesh and q-mesh of $(72 \times 72 \times 1)$ and $(9 \times 9 \times 1)$, respectively, according to convergence test.

Because a Ga atom is in s^2p^1 valence state, an isolated h-Ga sheet is not stable as it violates the aromatic rule. In this regard, one should introduce electrons into h-Ga to stabilize it. Motivated by the synthesis of a family of graphitic intercalation compounds and previous works on transition metal boride,[18] we use Hf atoms to inject electrons [Fig. 1(a)]. We first perform geometric optimizations and find that the Hf atoms prefer to adsorb on the hollow site of h-Ga, rather than the bridge site or top site. The relaxed geometry contains a single layer Hf sheet intercalated into two h-Ga layers, forming a sandwich Ga_2-Hf-Ga_2 system. The structure belongs to *P6/mmm* layer group with optimized lattice constants $a = b = 4.42$ Å. The atomic Wyckoff positions are 4*e* (1/3, 2/3, z_0) for Ga and 1*a* (0, 0, 0) for Hf, where $z_0 = 1.42$ Å is the vertical distance between the Ga and Hf layer. The bond length for Ga-Hf and Ga-Ga are 2.92 and 2.55 Å, respectively. The formation energy E_f $[= (E_{HfGa4} - 4\mu_{Ga} - \mu_{Hf})/5]$ is calculated to be 70 meV/atom. Here, μ_{Ga} and μ_{Hf} are the chemical potential of Ga and Hf, respectively, which are taken from the cohesive energy of the ground state phase of Ga and Hf, namely, α-Ga and *hcp*-Hf, respectively. Note that in the 3D binary Ga-Hf alloy the lowest formation energy is −664 meV/atom in Ga_3Hf_2,[19] which indicates that our 2D Ga_2-Hf-Ga_2 is a metastable structure. It has been postulated and experimentally confirmed that nanosheets with formation energy smaller than 200 meV/atom are likely to exist in free standing state.[20] Therefore, realizing that proposed $HfGa_4$ system is thermodynamically feasible. Our Bader's charge analysis[21] shows that each Hf donates ∼1.10 electrons.

Figure 1(b) shows the calculated phonon property. The absence of imaginary frequencies demonstrates that the material is dynamically stable. The calculated vibrational modes at the BZ center are shown in Fig. S1 of supplementary material.[22] One may wonder if lower concentration of Hf intercalation is possible. We also performed phonon calculation for Ga_6-Hf_2-Ga_6, where we find that it is dynamically unstable (Fig. S2).[22] This is also consistent with the above electron counting analysis. Hence, hereafter we will only focus on the Ga_2-Hf-Ga_2 system.

The calculated band structure of $HfGa_4$ is shown in Fig. 2(a). We see that $HfGa_4$ is a nonmagnetic metal. Most interestingly, one observes two linearly dispersive bands crossing each other along the Γ → K path [at the positions equivalent to $\Delta = (0.21, 0.21, 0) \times 2\pi/a$], forming six Dirac points in the first BZ. These Dirac points are located 68 meV below the E_F. We plot the 3D band profile near the Δ point in Fig. 2(c), which clearly shows a Dirac cone structure in 3D space. Detailed analysis reveals that these Dirac cones are anisotropic (Fig. S3).[22] We calculated the projected density of states and find that these Dirac cones are mainly contributed by Hf-e_2 orbital. This has been also confirmed by calculating the maximally localized Wannier function (MLWF)[23] of the Dirac cones [Figs. 2(e) and 2(f)] using the Wannier90 code.[24]

In order to understand the electron delocalization behavior, we calculate the valence electron localization function (ELF).[25,26] We see that in the Hf layer the delocalized electrons are distributed around the center of triangles formed by three Hf atoms, and the Hf sites have low electron density. In the Ga layer, the electrons are more delocalized around the Ga atoms (Fig. S4).[22]

Now we turn on SOC interaction. As shown in Fig. 2(b), one clearly sees that the band I and band II opens a gap at

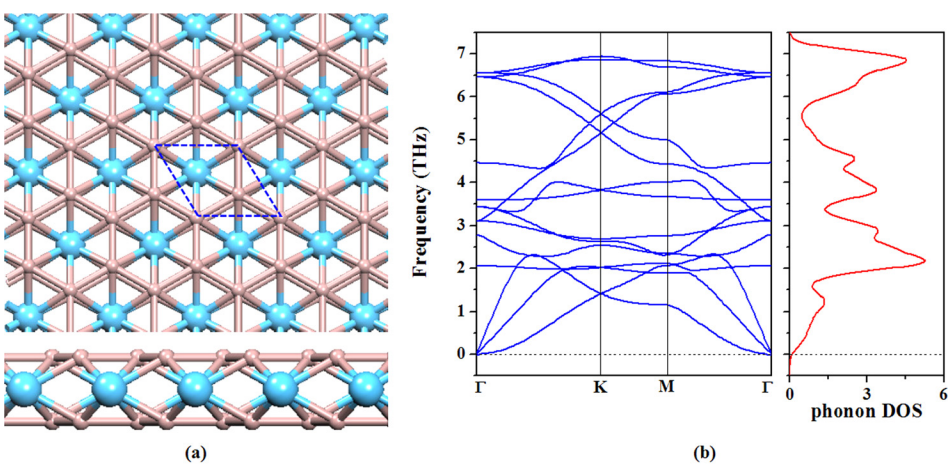

FIG. 1. (a) Structure (top view and side view) and (b) phonon spectra of Hf intercalated Ga compound.

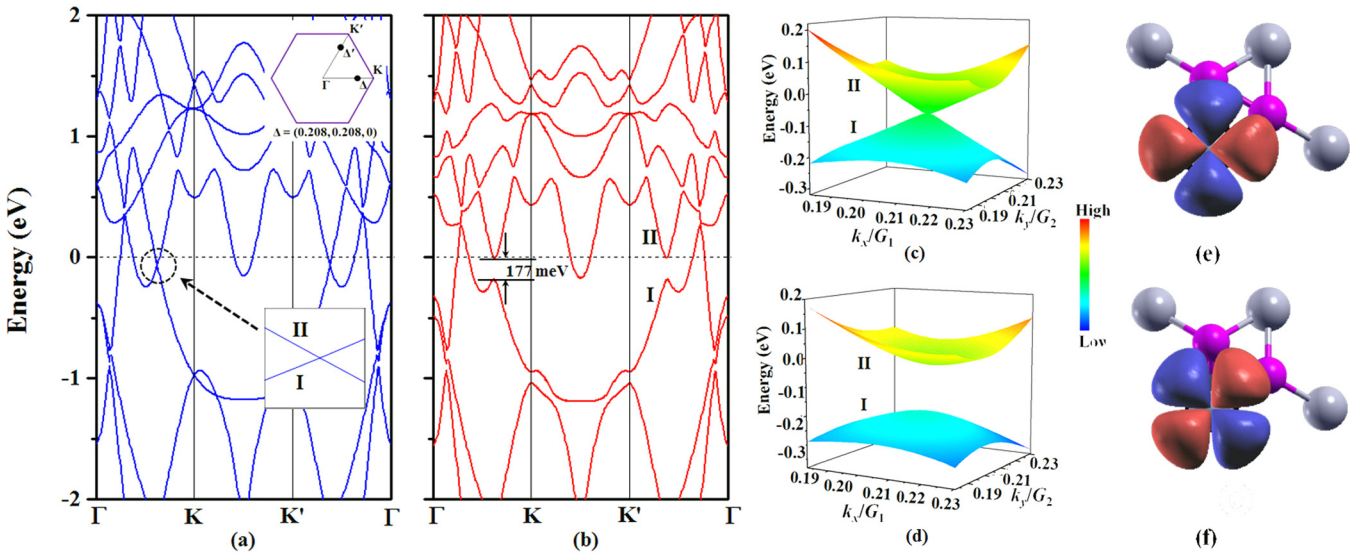

FIG. 2. (a) and (b) Band dispersion along the high symmetry path in the BZ, without and with SOC interaction, respectively. (c) and (d) represent band dispersion near Δ, without and with SOC, respectively. The MLWF of the Dirac cone bands are shown in (e) and (f).

the Dirac point Δ. The maximum of band I is located at $E_F - 181$ meV, and the minimum of band II is located at $E_F - 4$ meV, resulting in a large band gap of 177 meV. This value is much larger than that of similar structures MoB_4[18] and TiB_2,[27] and is large enough to be observed at room temperature. The 3D band profile of band I and band II is shown in Fig. 2(d). Note that at the E_F, the metallic character still remains. Such SOC induced band gap opening suggests a topologically nontrivial band character inside the gap. We also verify the band structure by using HSE06 treatment of exchange-correlation potential (Fig. S5).[28,29] We see that the HSE06 only results in a shift of band energies. The Dirac cone is located at the same Δ point as in the PBE results and lies 0.21 eV below the E_F. Furthermore, the HSE06 + SOC calculation shows a band gap of 282 meV.

To illustrate the detailed mechanism of band gap opening, we reproduce band I and II dispersions by employing a simplified tight binding (TB) model composed of d_{xy} and d_{x2-y2} orbitals. The Hamiltonian can be written as

$$\hat{H} = \sum_{\langle i,j\rangle,\alpha\beta} t_{i,\alpha}^{j,\beta}(\hat{c}_{i,\alpha}^{+}\hat{c}_{j,\beta} + \text{h.c.}) + t_{\text{SO}} \sum_{i,\alpha\beta} \langle \vec{L}\cdot\vec{\sigma}\rangle_{i,\alpha\beta},$$

where $c^{\dagger}_{i,\alpha}$ ($c_{i,\alpha}$) is the creation (annihilation) operator of an electron at site-i and orbital-α (=d_{xy} and d_{x2-y2}). L and σ are the angular momentum operator and the Pauli matrix, respectively. Figure S6 shows the TB results.[22] One can see that it reproduces the main features of the DFT results. Without SOC interaction, we observe Dirac point along the Γ → K path [at the point of $(0.19,\ 0.19,\ 0)\times 2\pi/a$]. When the SOC is switched on, these Dirac points open band gaps.

The Δ points are not located at the time-reversal-invariant momenta of BZ. This implies that they may be protected by crystal symmetry, instead of time reversal symmetry. As the $GaHf_4$ is symmetric under the reflection M, the eigenstates can be classified into different mirror eigenvalues, $+i$ and $-i$. To characterize the topological properties, we calculate the Berry curvatures associated with $+i$ and $-i$ mirror eigenstates

$$\Omega_{\pm i}(\mathbf{k}) = -2\sum_{E_{n,\mathbf{k}}\le\mu}\sum_{n'\neq n}\frac{\text{Im}\langle\psi_{n,\mathbf{k}}^{\pm i}|\hat{v}_x|\psi_{n',\mathbf{k}}^{\pm i}\rangle\langle\psi_{n',\mathbf{k}}^{\pm i}|\hat{v}_y|\psi_{n,\mathbf{k}}^{\pm i}\rangle}{(E_{n,\mathbf{k}}-E_{n',\mathbf{k}})^2}.$$

We move the chemical potential μ downward inside the band gap (at $E_F - 0.1$ eV). As shown in Fig. 3(a), we see that both Berry curvatures (Ω_{+i} and Ω_{-i}) are strongly concentrated in the vicinity of Δ points, and have opposite sign. Hence the total Chern number is zero. By numerically integrating the Ω_{+i} and Ω_{-i}, we obtain a nearly quantized nonzero mirror Chern number $C_M \sim -2$. This clearly demonstrates that the band gaps at Δ and its equivalent points are topologically protected by its mirror symmetry.

As the z-component of spin polarization is proportional to the mirror eigenvalue, we can expect a quantized spin current inside the nontrivial band gap. To examine this, we quantitatively calculate the z-component of spin Berry curvature

$$\Omega^{\text{SH}}(\mathbf{k}) = -2\sum_{E_{n,\mathbf{k}}\le\mu}\sum_{n'\neq n}\frac{\text{Im}\langle\psi_{n,\mathbf{k}}|\hat{j}_x|\psi_{n',\mathbf{k}}\rangle\langle\psi_{n',\mathbf{k}}|\hat{v}_y|\psi_{n,\mathbf{k}}\rangle}{(E_{n,\mathbf{k}}-E_{n',\mathbf{k}})^2},$$

where j_x is the spin current operator taking the form $(s_z v_x + v_x s_z)/2$. We see that the $\Omega^{\text{SH}}(\mathbf{k})$ has a small positive value around Γ, and has pronounced negative peaks at the Δ and its symmetry equivalent points [Fig. 3(b)]. This implies a nonzero in-plane intrinsic spin Hall conductance σ^{SH} within this band gap. We integrate the $\Omega^{\text{SH}}(\mathbf{k})$ to obtain the spin Hall conductivity $\sigma^{\text{SH}} = \frac{e^2}{4\pi\hbar}\int_{\text{BZ}}\Omega^{\text{SH}}(\mathbf{k})d^2\mathbf{k}$, where a factor of $2e/\hbar$ is multiplied to σ^{SH} to convert its unit into the conventional electron conductivity e^2/h.[30] Figure 3(c) shows the chemical potential dependence of σ^{SH}. We see a nearly quantized plateau inside the SOC band gap, taking the value of around $-4\ e^2/h$, and the magnitude of σ^{SH} decreases rapidly outside this band gap range.

The intrinsic (without electron or hole doping) $HfGa_4$ is a metal. We plot its Fermi surface (FS) geometry in k-space [Figs. 4(a) and 4(b)]. The SOC has marginal influence on the structure of the FS. Therefore, in order to reduce

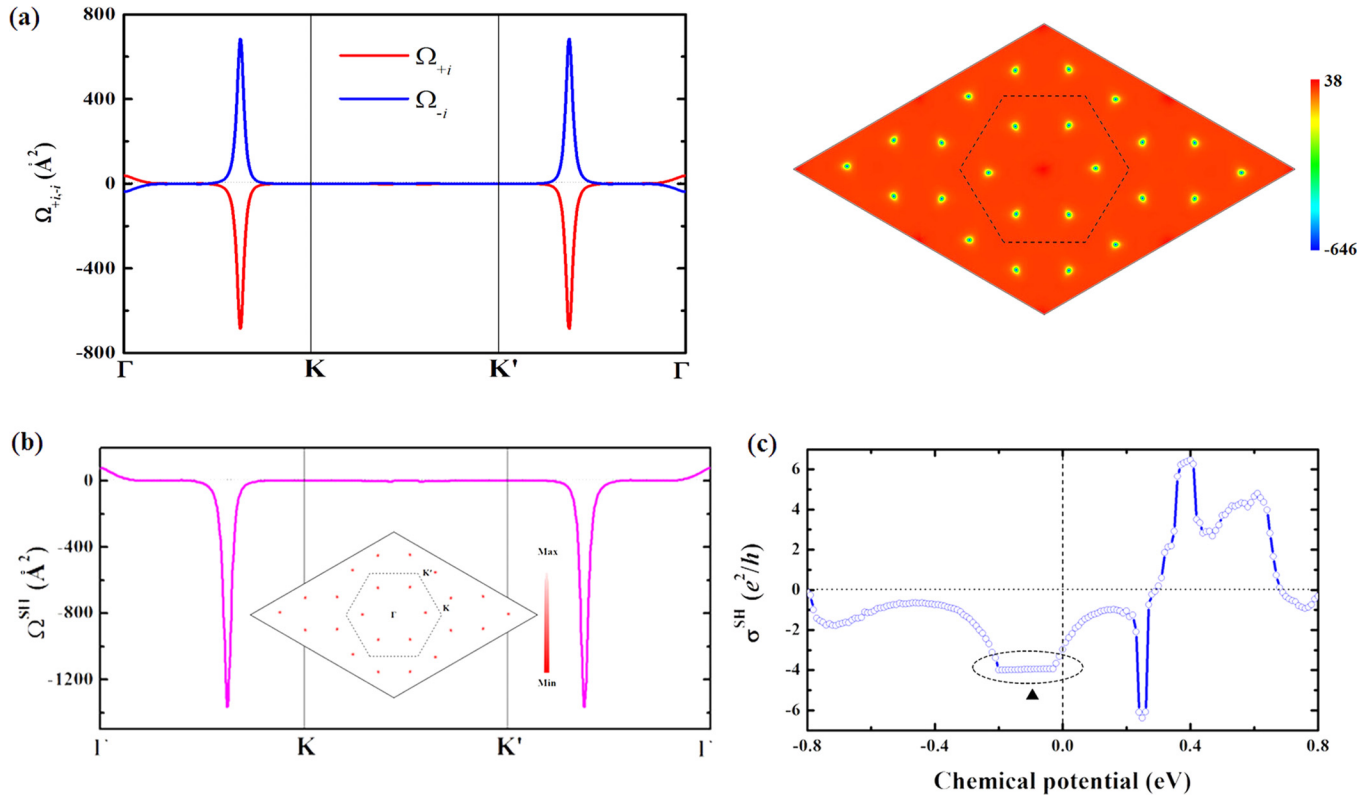

FIG. 3. (a) (Left panel) Berry curvature associated with $+i$ and $-i$ mirror eigenstates along the high-symmetry path. (Right panel) Distribution of Berry curvature associated with $+i$ mirror eigenstates over the whole 2D BZ. (b) k-resolved spin Berry curvature Ω^{SH} along the high symmetry path and (inset) in the BZ. (c) Integrated QSH conductance σ^{SH} with respect to chemical potential. The quantized terrace of σ^{SH} is highlighted by the dashed oval shape. The solid black triangle denotes the $\mu = E_F - 0.1$ eV.

computational costs, we discuss its FS and metallic character without including SOC. One clearly sees a distorted hexagonal ring pocket around the Γ point, contributed by Ga-s and Hf-e_2 orbitals. The nesting function, $\chi_{\mathbf{q}} = \sum_{\mathbf{k},m,n} \delta(E_{m,\mathbf{k}+\mathbf{q}} - E_F)\delta(E_{n,\mathbf{k}} - E_F)$, is calculated to reveal the interactions between electrons at different $\mathbf{k}$ on the FS [Fig. 4(c)]. We see that high $\chi_{\mathbf{q}}$ values appear around the central part of the first BZ, while on the edge of the BZ $\chi_{\mathbf{q}}$ is very small.

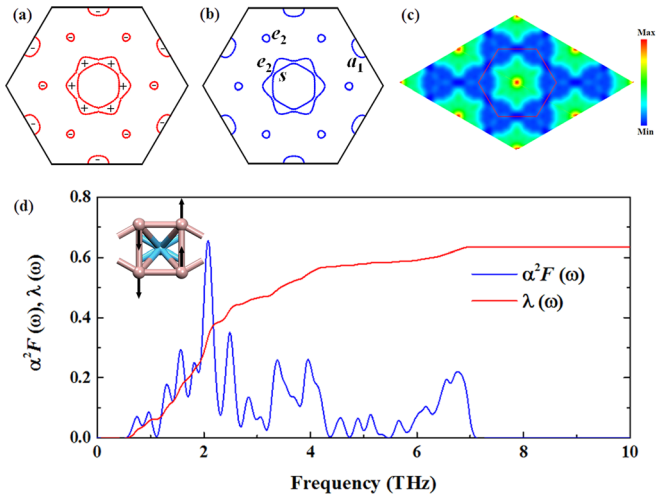

FIG. 4. k-resolved Fermi surface (a) without and (b) with SOC. "+" and "−" represent hole and electron pockets, respectively. In (b) we denote the dominant contributing orbital of Fermi pockets. (c) The nesting function. (d) Eliashberg function $\alpha^2F(\omega)$ and EPC parameter $\lambda(\omega)$. Inset shows the dominant vibrational mode contributing to EPC.

The large area of nonzero $\chi_{\mathbf{q}}$ motivates us to calculate the EPC interaction and Eliashberg function

$$\alpha^2F(\omega) = \frac{1}{2N_{\mathbf{q}}}\sum_{\mathbf{q},\nu}\gamma_{\mathbf{q}\nu}\delta(\omega - \omega_{\mathbf{q}\nu})/\omega_{\mathbf{q}\nu}\pi N_F$$

$$= \frac{1}{2N_{\mathbf{q}}}\sum_{\mathbf{q},\nu}\omega_{\mathbf{q}\nu}\lambda_{\mathbf{q}\nu}\delta(\omega - \omega_{\mathbf{q}\nu}),$$

where $\gamma_{\mathbf{q}\nu}$, $\lambda_{\mathbf{q}\nu}$, and $\omega_{\mathbf{q}\nu}$ are the phonon linewidth, partial EPC parameter, and phonon frequency of vibrational mode ν at $\mathbf{q}$, respectively. N_F is the DOS at the E_F. We find that the phonons at ~3.8 and ~6.5 THz around the Γ point have large phonon linewidth and EPC matrix element (Fig. S7). The Eliashberg function $\alpha^2F(\omega)$ and integrated EPC parameter $\lambda(\omega)$ are shown in Fig. 4(d). We see that the out-of-plane vibrational mode at ~2 THz contributes ~2/3 of the EPC parameter. Total value of λ is calculated to be 0.63, and the logarithmic frequency average $\omega_{\log}$ is 73.4 cm^{-1}. We estimate the transition temperature T_c by using Allen–Dynes modified McMillan equation,[31] $T_c = \frac{\hbar\omega_{\log}}{1.2k_B}\exp\left[\frac{-1.04(1+\lambda)}{\lambda-\mu*(1+0.62\lambda)}\right]$, with the effective Coulomb repulsion parameter μ* taking the usual value of 0.115. T_c is calculated to be 2.4 K. This demonstrates that the sandwich $HfGa_4$ is a BCS superconductor in its intrinsic state, adding a candidate to the Ga-based superconductor family.

In summary, we propose a stable Hf intercalated hexagonal Ga sandwich. We show that there are six symmetric Dirac cones, slightly below the Fermi level. When SOC interaction is included, all these Dirac cones open a large

band gap of 177 meV, which can be experimentally observed at room temperature. The mirror Chern number is calculated to be −2; thus, they are topologically nontrivial and protected by mirror, instead of time-reversal, symmetry. Such topological crystalline insulating phase is unusual in hexagonal lattice. We find a large QSH conductance $\sigma^{SH} \sim -4\ e^2/h$. Furthermore, our calculations reveal that the intrinsic state (no carrier doping) of the system has a high EPC interaction. We find that it is a BCS superconductor with T_c estimated to be 2.4 K. Therefore, we predict the coexistence of large band gap topological crystalline QSH effect and BCS superconducting state in a single nanomaterial, which can be manipulated by tuning its chemical potential within a small range.

This work is partially supported by grants from the U.S. Department of Energy, Office of Basic Energy Sciences, Division of Materials Sciences and Engineering under Award Nos. # DE-FG02-96ER45579 and # DE-FG02-11ER46827, and the National Natural Science Foundation of China (NSFC-51471004). This material is based upon work performed using computational resources supported by the University of Tennessee and Oak Ridge National Laboratory's Joint Institute for Computational Sciences (http://www.jics.utk.edu).[32] Any opinions, findings, and conclusions or recommendations expressed in this material are those of the author(s) and do not necessarily reflect the views of the University of Tennessee, Oak Ridge National Laboratory, or the Joint Institute for Computational Sciences.

The authors declare no competing financial interest.

[1]X.-L. Qi and S.-C. Zhang, Rev. Mod. Phys. **83**, 1057 (2011).
[2]L. Fu, Phys. Rev. Lett. **106**, 106802 (2011).
[3]Y. Okada, M. Serbyn, H. Lin, D. Walkup, W. Zhou, C. Dhital, M. Neupane, S. Xu, Y. J. Wang, R. Sankar *et al.*, Science **341**, 1496 (2013).
[4]Y. Tanaka, Z. Ren, T. Sato, K. Nakayama, S. Souma, T. Takahashi, K. Segawa, and Y. Ando, Nat. Phys. **8**, 800 (2012).
[5]J. Liu, T. H. Hsieh, P. Wei, W. Duan, J. Moodera, and L. Fu, Nat. Mater. **13**, 178 (2014).
[6]J. M. Lu, O. Zheliuk, I. Leermakers, N. F. Q. Yuan, U. Zeitler, K. T. Law, and J. T. Ye, Science **350**, 1353 (2015).
[7]J. Zhou, Q. Sun, Q. Wang, and P. Jena, Phys. Rev. B **90**, 205427 (2014).
[8]B. M. Ludbrook, G. Levy, P. Nigge, M. Zonno, M. Schneider, D. J. Dvorak, C. N. Veenstra, S. Zhdanovich, D. Wong, P. Dosanjh *et al.*, Proc. Natl. Acad. Sci. U.S.A. **112**, 11795 (2015).
[9]W. Xie, H. Luo, B. F. Phelan, T. Klimczuk, F. A. Cevallos, and R. J. Cava, Proc. Natl. Acad. Sci. U.S.A. **112**, E7048 (2015).
[10]H.-M. Zhang, Y. Sun, W. Li, J.-P. Peng, C.-L. Song, Y. Xing, Q. Zhang, J. Guan, Z. Li, Y. Zhao *et al.*, Phys. Rev. Lett. **114**, 107003 (2015).
[11]Y. Xing, H.-M. Zhang, H.-L. Fu, H. Liu, Y. Sun, J.-P. Peng, F. Wang, X. Lin, X.-C. Ma, Q.-K. Xue *et al.*, Science **350**, 542 (2015).
[12]L. Li, Y. Wang, S. Xie, X.-B. Li, Y.-Q. Wang, R. Wu, H. Sun, S. Zhang, and H.-J. Gao, Nano Lett. **13**, 4671 (2013).
[13]J. P. Perdew, K. Burke, and M. Ernzerhof, Phys. Rev. Lett. **77**, 3865 (1996).
[14]G. Kresse and J. Furthmüller, Phys. Rev. B **54**, 11169 (1996).
[15]P. E. Blöchl, Phys. Rev. B **50**, 17953 (1994).
[16]H. J. Monkhorst and J. D. Pack, Phys. Rev. B **13**, 5188 (1976).
[17]P. Giannozzi, S. Baroni, N. Bonini, M. Calandra, R. Car, C. Cavazzoni, D. Ceresoli, G. L. Chiarotti, M. Cococcioni, I. Dabo *et al.*, J. Phys.: Condens. Matter **21**, 395502 (2009).
[18]S.-Y. Xie, X.-B. Li, W. Q. Tian, N.-K. Chen, X.-L. Zhang, Y. Wang, S. Zhang, and H.-B. Sun, Phys. Rev. B **90**, 035447 (2014).
[19]O. Levy, G. L. W. Hart, and S. Curtarolo, Acta Mater. **58**, 2887 (2010).
[20]A. K. Singh, K. Mathew, H. L. Zhuang, and R. G. Hennig, J. Phys. Chem. Lett. **6**, 1087 (2015).
[21]E. Sanville, S. D. Kenny, R. Smith, and G. Henkelman, J. Comput. Chem. **28**, 899 (2007).
[22]See supplementary material at http://dx.doi.org/10.1063/1.4954672 for vibrational modes, geometric and phonon of low concentration intercalation, contour plot of band II, ELF, HSE06 and tight binding band structure, and EPC strength.
[23]N. Marzari, A. A. Mostofi, J. R. Yates, I. Souza, and D. Vanderbilt, Rev. Mod. Phys. **84**, 1419 (2012).
[24]A. A. Mostofi, J. R. Yates, Y.-S. Lee, I. Souza, D. Vanderbilt, and N. Marzari, Comput. Phys. Commun. **178**, 685 (2008).
[25]A. D. Becke and K. E. Edgecombe, J. Chem. Phys. **92**, 5397 (1990).
[26]A. Savin, O. Jepsen, J. Flad, O. K. Andersen, H. Preuss, and H. G. von Schnering, Angew. Chem., Int. Ed. **31**, 187 (1992).
[27]L. Z. Zhang, Z. F. Wang, S. X. Du, H. J. Gao, and F. Liu, Phys. Rev. B **90**, 161402 (2014).
[28]J. Heyd, G. E. Scuseria, and M. Ernzerhof, J. Chem. Phys. **118**, 8207 (2003).
[29]J. Heyd, G. E. Scuseria, and M. Ernzerhof, J. Chem. Phys. **124**, 219906 (2006).
[30]W. Feng, Y. Yao, W. Zhu, J. Zhou, W. Yao, and D. Xiao, Phys. Rev. B **86**, 165108 (2012).
[31]P. B. Allen and R. C. Dynes, Phys. Rev. B **12**, 905 (1975).
[32]M. R. Fahey, R. Budiardja, L. Crosby, and S. McNally, "Deploying Darter – A Cray XC30 System," in *29th International Conference, ISC 2014*, Lecture Notes in Computer Science, edited by J. M. Kunkel, T. Ludwig, and H. W. Meuer (Springer International Publishing, Switzerland, 2014), Vol. 8488, pp. 430–439.

Supplemental Material

Integrating superconducting phase and large topological crystalline quantum spin Hall effect in hafnium intercalated gallium film

Jian Zhou,[1] Shunhong Zhang,[2] Qian Wang,[2,3,1] Puru Jena[1]

[1] *Department of Physics, Virginia Commonwealth University, Richmond, VA 23284, USA*

[2] *Center for Applied Physics and Technology, College of Engineering, Peking University, Beijing 100871, China*

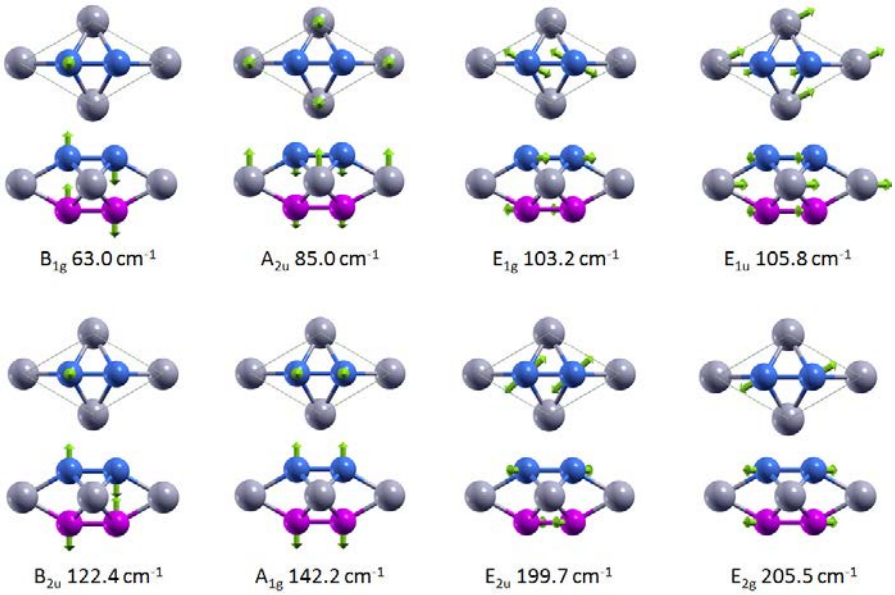

FIG. S1 Vibrational modes of optical branches at the Γ point. Both the top and side views are shown. For clarity the top and bottom layer of Ga are denoted by blue and magenta spheres, respectively. Hf atoms are represented by grey spheres. Atomic vibration magnitude and direction are displayed by the length and orientation of green arrows.

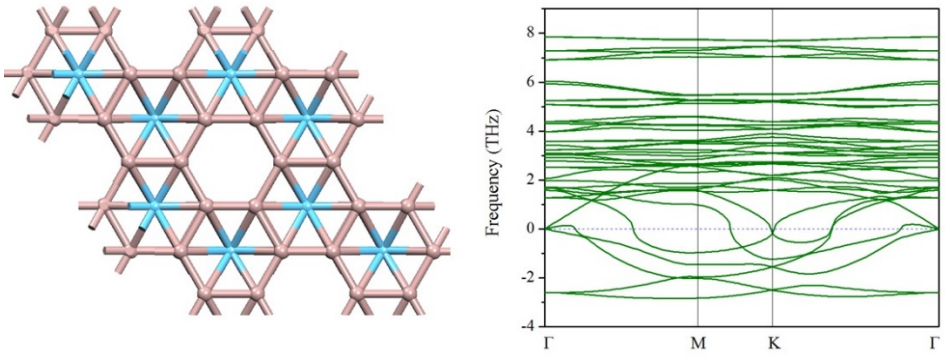

FIG. S2 Geometric structure of lower concentration (Ga_6-Hf_2-Ga_6) and its phonon dispersion. One clearly sees that the low concentration is dynamically unstable due to its inconsistent with the electron counting analysis discussed in the main text.

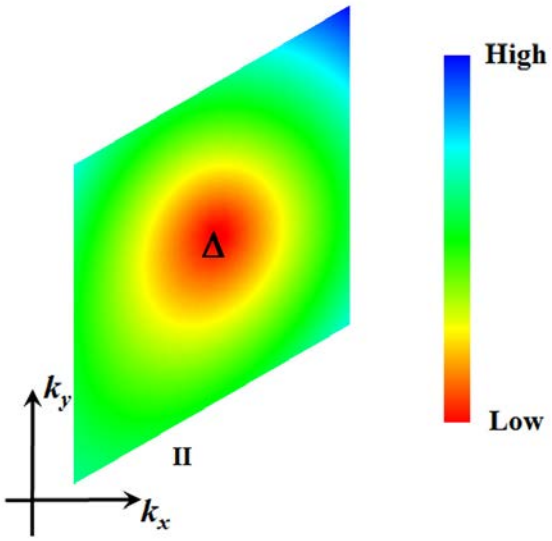

FIG. S3 Contour plot of the band II around the Δ point, where one sees a clear anisotropic feature.

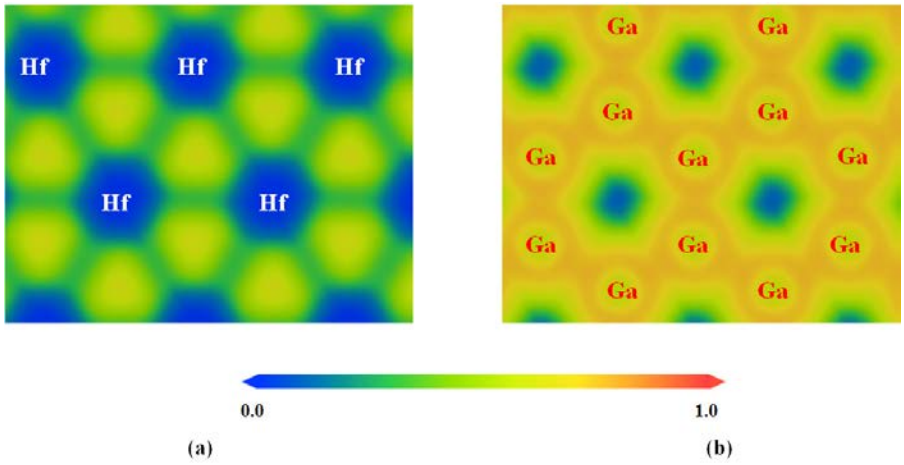

FIG. S4 Slice form of ELF crossing (a) Hf layer and (b) Ga layer.

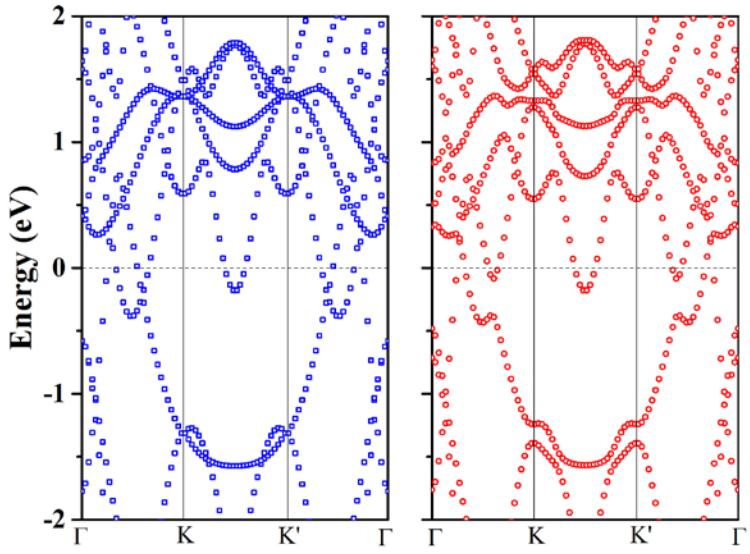

FIG. S5 Band structures calculated by (left) HSE06 and (right) HSE06+SOC.

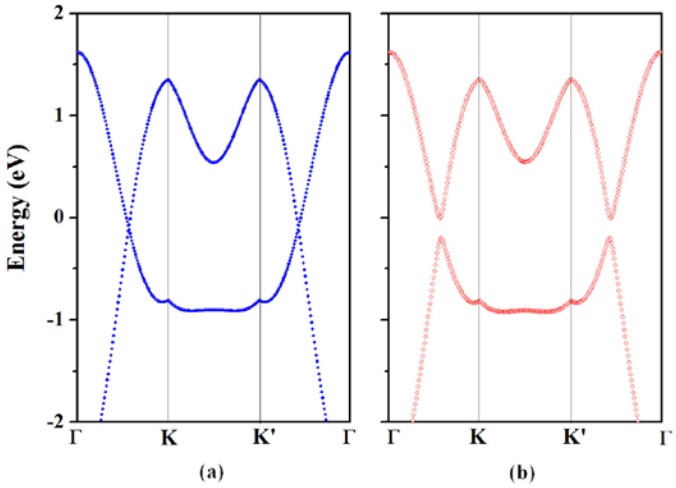

FIG. S6 Tight binding band dispersion results. The Hamiltonian can be seen in the main text. The hopping integral parameters between orbitals are $t_{dxy.\mathrm{vs}.dxy} = t_{dx2\text{-}y2.\mathrm{vs}.dx2\text{-}y2} = -0.18$ eV, $t_{dxy.\mathrm{vs}.dx2\text{-}y2} = t_{dx2\text{-}y2.\mathrm{vs}.dxy} = -0.36$ eV. In panel (a) one observes Dirac-points along the Γ→K path, slightly below the E_F. In panel (b) we include SOC with $t_{SO} = 0.05$ eV, where a band gap of ~180 meV is open.

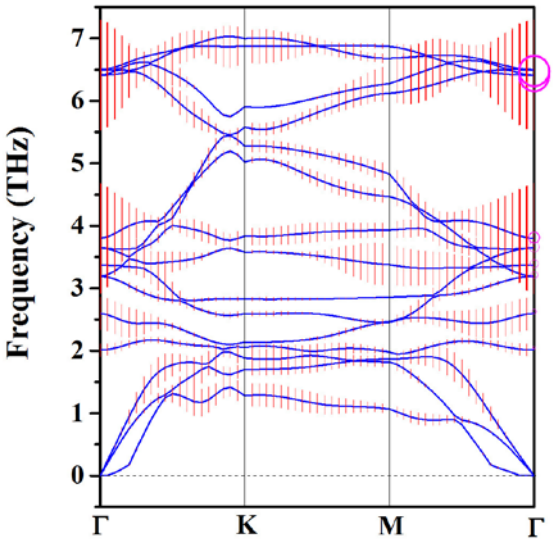

FIG. S7 EPC phonon dispersion. Red bars show the phonon linewidth $\gamma_{\mathbf{q}\nu}$ (the magnitude is increased to be 1000 times). Pink circles are proportional with EPC matrix element at Γ.